TUHH
Hamburg
University of
Technology

UKE

Comprehensive Guidelines and Templates for Thesis Writing

Master's Thesis

of

Author

Date of issue:
Date of submission:
Examiner:
Supervisor:

Statutory Declaration

I, Author, hereby affirm that the following Master's thesis has been elaborated solely by myself. No other means and sources except those stated, referenced and acknowledged have been used.

(Author)

Abstract

Contents

Acronyms Index

TUHH: Hamburg University of Technology
SOFA: Sequential Organ Failure Assessment
qSOFA: Quick Sequential Organ Failure Assessment
ICU: Intensive Care Unit
EHR: Electronic Health Record
YAIB: Yet Another ICU Benchmark
FSQ: Finite Scalar Quantization
SI: Suspected Infection
ABX: Antibiotics
DNM: Dynamic Network Model
LDM: Latent Dynamics Model
ML: Machine Learning
DL: Deep Learning
ODE: Ordinary Differential Equation
JIT: Just In Time Compilation
GPU: Graphics Processing Unit
PID: Proportional-Integral-Derivative
SIRS: Systemic Inflammatory Response Syndrome
PAMP: Pathogen-Associated Molecular Patterns
DAMP: Damage-Associated Molecular Patterns
PRR: Pattern Recognition Receptors
GLM: Generalized Linear Model
BCE: Binary Cross Entropy

1 List of Notes

- Sections to ChaptersStylingAppendix to real AppendixFix ACR separationFix newline/ linebreak after HeadingsSources misc + link 12
- actual functional model what is learned connecting parts 12
- can we fix please? 16
- correct source 18
- cite 23
- End this 23
- cite 27
- Figure bio vs oscillators 28
- why no ref? 29
- left out superscripts for better readability 30
- schreiben 31
- Non breakable tables? 32
- index for immune 33
- K colorbar 35
- which is stronger? 35
- not a sequence 37
- format 39
- ref sections 39
- Fix the edges 43
- table 43
- How to structure the latent space? Binary classification (sepsis, no sepsis) may not provide enough information to accurately structure the latent space. The options : Add more classes like resilient/vulnerable… maybe even the full spectrum? need to be modeled by R 44
- mapping not really clear, which metrics correspond to sofa/infection 44
- YAIB and other resources care about the onset of infection and sepsis . For sepsis this isn t really problematic since we could use the state transitions as indicators. But for the suspected infection it is problematic, maybe use si _upr and si _lwr provided by (https://eth-mds.github.io/ricu/reference/label_si.html). These would be 48h - SI - 24h adapted from , maybe a bit too much. 44

- Sections to Chapters
- Styling
- Appendix to real Appendix
- Fix ACR separation
- Fix newline/linebreak after Headings
- Sources misc + link

actual functional model what is learned connecting parts

2 Introduction

3 Medical Background (Sepsis)

As the most extreme course of an infectious disease, sepsis poses a very serious health threat, with a high mortality rate and frequent long-term consequences for survivors. In 2017, an estimated 48.9 million people worldwide suffered from sepsis and the same year, 11.0 million deaths were associated with sepsis [1], which makes up 19.7% of yearly deaths, making it the most common cause of in-hospital deaths. Untreated, the disease is always fatal and even with successful treatment, around 40% of those affected suffer long-term consequences, such as cognitive, physical or physiological problems, the so called *post-sepsis syndrome* [2]. Overall, treated and untreated septic diseases in particular represent an enormous burden on the global healthcare system. The observed risk of mortality significantly differs between lower to middle income countries with $> 50\%$ and high income countries with $< 25\%$.

Even though almost half of all sepsis-related deaths occur as a secondary complication of an underlying injury or a non-communicable, also known as chronic disease [3], the underlying triggers but also the individual progressions of sepsis remain highly diverse and heterogeneous. Moreover, a septic condition can not be reduced to a single specific physiological phenomenon, instead it combines multiple complex and interdependent processes across different biological scales.

This complexity has historically made it difficult to define sepsis in a medical precise way compared to other conditions. Multiple definitions have been proposed over time, and the terminology around sepsis and septic-shocks has often been blurry. The most commonly used and accepted sepsis definition characterizes sepsis as a "life-threatening organ dysfunction caused by a dysregulated host response to infection" [4]. The following Section 3.1 provides a detailed overview to this definition, which is referred to as Sepsis-3. Furthermore, Section 3.2 introduces the both the pathology and underlying biology of sepsis in greater detail.

A recent study [5] highlights the importance of early recognition and subsequent treatment of infections in patients, reducing the mortality risk caused from sepsis. Each hour of earlier detection can significantly increase the chance of survival [5], it urges to develop accurate and robust detection and prediction methods, i.e. reducing the time to receive the appropriate medical attention. In Section 3.3 the necessity for reliable and clinically practical sepsis prediction systems is discussed.

3.1 The Sepsis-3 Definition

Earlier definitions (Sepsis-1, Sepsis-2 [6]) primarily emphasized Systemic Inflammatory Response Syndrome (SIRS) [6] criteria, focusing on the inflammatory origins of sepsis. These definitions were later criticized for low specificity and under-representation of the multi organ failure due to sepsis. Out of the need for an update of these outdated definitions and partly

misleading sepsis models a task force led by the "Society of Critical Care Medicine and the European Society of Intensive Care Medicine", was formed in 2016. Their resolution, named "Third International Consensus Definitions for Sepsis and Septic Shock" [4], provides until today the most widely used sepsis definition and guidance on sepsis identification.

In general, sepsis does not classify as a specific illness, rather a multifaceted condition of "physiologic, pathologic, and biochemical abnormalities" [4], and septic patients are largely heterogeneous. Also the trigger is explicitly non-specific, since different triggers can cause the same septic condition. Most commonly the underlying cause of sepsis is diarrhoeal disease, road traffic injury the most common underlying injury and maternal disorders the most common non-communicable disease causing sepsis [1].

According to the Sepsis-3 definition, a patient is in a septic condition if the following two criteria are fulfilled:

- a documented or Suspected Infection (SI) and
- the presence of a dysregulated host response

The combination of the two criteria represents an exaggerated immune reaction that results in organ dysfunction, when infection is first suspected, even modest organ dysfunction is linked to a 10% increase of in-hospital mortality. A more pathobiological explanation of what a "dysregulated host response" means is given in the next Section 3.2.

Confirmed or Suspected Infection has no strict medical definition and classification what counts as SI remains a little vague, ultimately it is left for the medical personnel to classify infections or the suspicion of infections. For retrospective data-driven classification it is suggested to characterize any patient prescribed with Antibiotics (ABX) followed by the cultivation of body fluids, or the other way around, with a SI [4]. The timings of prescription and fluid samplings play a crucial role. If the antibiotics were administered first, then the cultivation has to be done in the first 24h after first prescription, if the cultivation happened first, the ABX have to be prescribed in the following 72h [4]. This can be seen in the lower part of figure Figure 1, with the abbreviated ABX. Regardless which happened first, the earlier of the two times is treated as the time of suspected infection onset time.

Dysregulated Host Response is characterized by the worsening of organ functionality over time. Since there is no gold standard for measuring the amount of "dysregulation" the Sepsis-3 consensus relies on the Sequential Organ Failure Assessment (SOFA)-score introduced in ([4], [7]). The score is now regularly used to evaluate the functionality of organ systems and helps to predict the risk of mortality, also outside of a sepsis context. The SOFA score is calculated at least every 24 hours and assess six different organ systems by assigning a score from 0 (normal function) to 4 (high degree of dysfunction) to each. The overall score is calculated as sum of each individual system.

can
we fix pleas

It includes the respiratory system, the coagulation/clotting of blood, i.e. changing from liquid to gel, the liver system, the cardiovascular system, the central nervous system and the renal system/kidney function. A more detailed listing of corresponding markers for each organ assessment can be found in table Table 4 in the Section 11. The magnitude of a patients initial SOFA-score captures preexisting organ dysfunction. An increase in SOFA score ≥ 2 corresponds to an acute worsening of organ functionalities and a drastic worsening in the patients condition, the indicator for a dysregulated response.

3.1.1 Sepsis Classification

The Sepsis-3 definition not only provides the clinical criteria of septic conditions, but also introduces the necessary time windows for sepsis classification. An increase of SOFA ≥ 2 in the 48h before or 24h after the SI time, the so called SI-window, is per Sepsis-3 definition the "sepsis onset time". A schematic of the timings is shown in figure Figure 1.

With respect to which value the increase in SOFA is measured, i.e. the baseline score, is not clearly stated in the consensus and leaves room for interpretation, commonly used approaches include:

- the minimal value inside the SI-window before the SOFA increase,
- the first value of the SI-window,
- the lowest value of the 24h previous to the increase.

Differences in definitions greatly influence the detection of sepsis, which are used for prevalence estimates for example [8]. Using the lowest SOFA score as baseline, the increase ≥ 2 for patients with inspected infection was associated with an 18% higher mortality rate according to [7] a retrospective Intensive Care Unit (ICU)-data analysis.

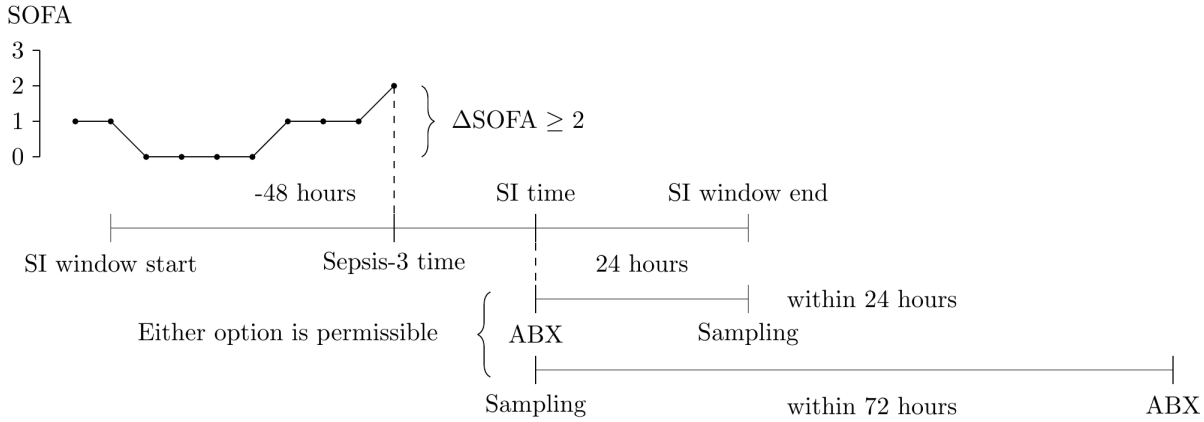

Figure 1: Graphical representation of the timings in the Sepsis-3 definition, taken from [9]

Up until today, even though SOFA was created as a clinical bedside score, some of the markers used in it are not always available to measure or at least not at every 24h [10]. For a faster bedside assessment [7] also introduced a clinical score termed Quick Sequential Organ Failure Assessment (qSOFA), with highly reduced marker number and complexity, it includes:

- Respiratory rate ≥ 22/min
- Altered mentation
- Systolic blood pressure ≤ 100 mmHg

Patients fulfilling at least two of these criteria have an increased risk of organ failure. While the qSOFA has a significantly reduced complexity and is faster to assess it is not as accurate as the SOFA score, meaning it has less predictive validity for in-house mortality [7].

There is also the notion of a septic shock, also defined in [4], which an in-hospital mortality above 40%. Patients with a septic shock are can be identified by:

- Sepsis
- Persisting hypotension requiring
  vasopressors to maintain MAP $\geq$ 65mmHg
- Serum lactate level > 2 mmol/L, despite volume resusciation.

3.2 Biology of Sepsis

This part tries to give an introduction into the biological phenomena that underlie sepsis. Starting with an explanation on how human tissue is reacting to local infections or injuries on a cellular level in Section 3.2.1 and how this can escalate to *cytokine storms* in Section 3.2.2 and ending with systemic organ failure in Section 3.2.3.

Certain details and specifities are left out when not essential for the understanding of this project. More detailed explanations can be found in the primary resources provided throughout this section.

3.2.1 Cellular Origins

Human organ tissue can be differentiated into two broad cell-families called *parenchymal* and *stroma* which are separated by a thin, specialized boundary layer known as the *basal lamina*.

The parenchymal cells perform the primary physiological functions of an organ, with every organ hosting distinct parenchymal cells [11].

Everything not providing organ-specific functionalities forms the stroma, that includes the structural or connective tissue, blood vessels and nerves. The stroma not only contributes to the tissues structure, but it also actively participates in biochemical signaling and immune regulation. This way it helps to maintain a healthy and balanced tissue, the *homeostasis*, and enables coordinated responses to injury or infection [12].

correct source

A pathogen is summarizes all types of organisms that can be harmful to the body, this includes germs, fungi, algae, or parasites. When a pathogen enters the body through the skin, a mucous membrane or an open wound, the first line of non-specific defense, the innate immune system [13], gets activated.

This rapid response does not require the body to have seen the specific pathogen before. Instead, the innate immune system can be triggered by sensing commonly shared features of pathogens, in case of germs known as Pathogen-Associated Molecular Patterns (PAMP), for injury called Damage-Associated Molecular Patterns (DAMP) [14]. The PAMP's and DAMP's can be detected by Pattern Recognition Receptors (PRR), which are found in resident immune cells, as well as stroma cells. Once a pathogen is detected a chain reaction inside the cell leads to the creation and release of signaling proteins called *cytokines* [15].

Cytokines are a diverse group of small signaling proteins which play a special role in the communication between other cells, both neighboring and across larger distances through the bloodstream. They are acting as molecular messengers that coordinate the recruitment of circulating immune cells and will guide them to the location of infection or injury [15].

Besides their role in immune activation where cytokines regulate the production of anti- and pro-inflammatory immune cells which help with the elimination of pathogens and trigger the healing process right after. They are also participating in the growing process of blood cells.

One specialty of these relatively simple proteins is that they can be produced by almost every other cell, with different cells being able to produce the same cytokine. Further, cytokines are redundant, meaning targeted cells can show identical responses to different cytokines [16], these features seems to fulfill some kind of safety mechanism to guarantee vital communication

flow. After release cytokines have relatively a short half-life (only a few minutes) but through cascading-effects the cytokines can have substantial impact on their micro-environment.

3.2.2 Cytokine Storms

The hosts dysregulated response to an infection connected to the septic condition is primarily driven by the excessive and uncontrolled release cytokines and other mediators. Under normal circumstances, the release of inflammatory cytokines tightly regulated in time and magnitude. After the pathogen detection the release is quickly initiated, peaks as immune cells are recruited and automatically fades out once the initial pathogen is controlled and the host returns to a healthy and balanced state, the homeostasis.

In certain scenarios a disturbance to the regulatory mechanisms triggers positive inflammatory feedback loop, followed by a massive release of pro-inflammatory cytokines. These cells further activate additional immune and non-immune cells, which in turn amplify the cytokine production, creating a self-reinforcing cycle of immune activation [17]. This ultimately leads to a continuous and uncontrolled release of cytokines that fails to shut down. With this overreaction, called *cytokine storm*, the immune response and release of inflammatory mediators can damage the body more than the infection itself.

Although the quantity of cytokines roughly correlates with disease severity, concentrations of cytokines vary between patients, time and even different body-parts, making a distinction between an appropriate reaction and a harmful overreaction almost impossible [17]. Out of all cytokines, only a small subset or secondary markers can be measured through blood samples to detect increased cytokine activity. This limited accessibility cytokines difficult to study in general, they prove to be little useful as direct indicators of pathogenesis or diagnostic purposes.

Since the 90s there has been a lot of research focused on cytokines and their role in the innate immune system and overall activation behavior. Multiple therapeutic interventions have been tested in clinical trials, yet none have achieved a significant improvement in survival outcomes [14]. This emphasizes the complexity of sepsis as a systemic syndrome rather than a single-cause disease, and suggests that cytokine storms are an emergent property rather than the result of any one molecular trigger. To this day, the fundamental principles that govern the transition from a regulated immune response to a self-destructive cytokine storm remain not fully understood.

3.2.3 Systemic Consequences and Organ Failure

While more and more cytokines are released, they flood not only infected areas, but also surrounding parts of the tissue and circulation, causing localized inflammatory response to become systemic. The widespread cytokine reaction starts to disrupt the normal metabolism of parenchymal cells in organs due to a deficiency in oxygen and nutrients.

To compensate, cells switch from their usual oxygen-based metabolism to an *anaerobic glycolysis* [18], generating energy less efficiently from glucose. As a result, metabolic by-products such as lactate accumulate making the surrounding environment more acidic, which further harms the cells and leads to more cellular dysfunction.

At the same time, the mitochondria, the “power house” of the cells, start to fail. The walls of blood vessels become leaky, allowing fluids to move into surrounding tissue. This causes swelling and lowers the blood pressure, which in turn reduces the oxygen supply even further [14].

Step by step, the death of cells spreads throughout the body and affects organ functionality. When multiple organs fail simultaneously, the condition becomes irreversible [4]. At this stage, multi-organ-failure is the final and most lethal form of sepsis, with each additional affected organ the mortality increases drastically.

3.3 The need for sepsis prediction

To this day sepsis, and the more extreme septic shock, remains as an extreme burden to the worldwide healthcare system. It is associated with high rates of incidence, high mortality and significant morbidity. Despite overall advancements in medical care and slowly decreasing prevalence numbers, sepsis continues to be the leading cause of in-hospital death [19].

In germany it was estimated in 2022 that at least 17.9% of intensive care patients develop sepsis, and 41.7% of all hospital treated sepsis patients die during their stay [3]. The economic burden is equally severe, with the annual cost of sepsis treatment in germany estimated to be €7.7 billion based on extrapolated data from 2013.

Globally , the situation is even more concerning, as sepsis remains to be under-diagnosed significantly due to its non-specific symptoms. Environmental and socioeconomic factors such as insufficient sanitation, limited access to clean water and healthcare increases the incidence particularly in low- to middle income countries [1], [19].

A meta-analysis of seven sepsis alert systems found no evidence for improvement in patient outcomes, suggesting insufficient predictive power of analyzed alert systems or inadequate system integration [20]. Nevertheless, positive treatment outcomes depend heavily on timely recognition and intervention [19]. Each hour of delayed treatment increases mortality risk, underscoring the critical importance of early detection [5] while structured screening and early warning systems have demonstrated reductions in time-to-antibiotics and improvements in outcomes [21]. These findings confirm that in principle earlier identification of sepsis improves clinical results, even if existing tools are not yet capable enough, and emphasizes the need for more research in that direction.

A recent study suggests a paradigm shift in sepsis detection—from a symptom-based to a systems-based approach [22]. Instead of waiting for clinical signs, early recognition should integrate multiple physiological and biochemical signals to capture the transition from infection to organ dysfunction. This aligns with the findings of a survey among clinicians regarding AI-Assistance in healthcare [23]. One participant emphasizes that specific vitals signs might be of less importance, rather the change/trend of a patients trajectory should be the prediction target. Another piece of finding of the same study was the preference of trajectories over plain binary event predictions.

However, implementation any data-driven prediction approaches into clinical practice presents challenges. Implementation studies consistently identify barriers such as alert fatigue, workflow disruption, and inconsistent screening uptake. To be effective, predictive systems must integrate seamlessly into and existing workflows provide interpretable output and aid the clinical expertise [23].

Taken together, these insights highlight both the need and the opportunity for improved sepsis prediction. The global burden and clinical urgency justify the development of more reliable prediction systems. At the same time, the limitations of current alert systems and implementation barriers underline the necessity for models that can integrate dynamic patient data and capture clinical trajectories.

4 Problem definition

This section provides some background on the specific research questions which are investigated in Section 9 using the methods introduced in Section 5 and Section 6 respectively. As discussed in Section 3.3, there is a substantial need for robust methods to identify patients sepsis onset and overall progression. This work provides a proof of concept for such a prediction system.

The increasing availability of high-quality medical data, i.e. multiple physiological markers with high temporal resolution, enables both classical statistical and Machine Learning (ML) (including Deep Learning (DL)) methods (see Section 7). While these purely data-driven approaches often achieve acceptable performance but the explainability of the prediction suffers and limits their adoption in clinical practice .

cite

In parallel, recent advances in the field of network physiology have introduced new ways to model physiological systems as interacting subsystems rather than isolated organs [24]. The Dynamic Network Model (DNM) introduced in [25] and adapted in [26], allows for a functional description of organ failure in sepsis and shows realistic system behavior in preliminary analysis. An in-depth introduction to the DNM is provided in Section 5. But up until now the dynamic model has not yet been verified on real data. The goal is to investigate how real patients would translate to the model parameters, and how the temporal physiological evolution can be incorporated and if there is a benefit doing so.

To summarize, the specific research questions include:

- **Usability of the DNM**: How and to what extent can the ML-determined trajectories of the DNM be used for detection and prediction, especially of critical infection states and mortality.
- **Comparison with data-based approaches**: How can the model-based predictions be compared with those of purely data-based approaches in terms of predictive power and interpretability.

End this

5 Model Background (Dynamic Network Model)

As outlined in Section 3, the macroscopic multi-organ failure associated with sepsis is driven by a dysregulated cascade of signaling processes on a microscopic level (see Section 3.2). This cascade involves a massive amount of interconnected components, where the connections mechanics and strengths vary over time and space. For example, these interactions differ across tissues and evolve as sepsis progresses, with crossing biochemical thresholds the behavior of cells can be changed [27].

In essence, cell-to-cell and cell-to-organ interaction in septic conditions form a highly dynamic, nonlinear and spatio-temporal network of relationships [28], which cannot be fully understood by a reduction to single time-point analyzes. Even though many individual elements of the inflammatory response are well characterized, we still fail to integrate them into a coherent system-level picture.

To address this complexity, the emerging field of *Network Physiology* provides a promising conceptual framework. Rather than studying components in isolation, network physiology focuses on the coordination and interconnection among the diverse organ systems and subsystems [24]. It enables the study of human physiology as a complex, integrated system, where emergent macroscopic dynamics arise from interacting subsystems that cannot be explained by their individual behavior. This perspective translates to the mesoscopic level, i.e. the in-between of things, where the coupling mechanisms collectively determine the overall physiological function.

In network physiology, the analytical basis of the bodies interacting systems is often graph based. Nodes represent subsystem such as organs or cell populations and links represent functional couplings or communication pathways [24]. Unlike classical graph theory, where dynamics are introduced by changing the graph topology (e.g. adding or removing links or nodes), in *Complex Networks* the links themselves can evolve dynamically in response to other system variables. These adaptive connections allow for information to propagate through the whole network, giving rise to emerging phenomena on global scales for otherwise identical network topologies.

Complex networks are well studied in physics and biology and have been applied to various physiological domains. Early works, such as [29] that have studied the cardiovascular system, while more recent studies have focused on the cardio-respiratory coupling [30] and large-scale brain network dynamics [31]. Network approaches have also provided mechanistic insights into disease dynamics, for example Parkinson [32] and Epilepsy [33], just to name a few.

Building on these interaction centric principles has opened up new opportunities to study how the inflammatory processes, such as those underlying sepsis, emerge from the complex inter- and intra-organ communication. In particular [25] and [26] have introduced a dynamical system

that models the cytokine behavior in patients with sepsis and cancer. This functional model will be referred to as Dynamic Network Model and forms the conceptual foundation for this whole project.

The remainder of this chapter is structured as follows: In Section 5.1 introduces the theoretical backbone of the DNM, the Kuramoto oscillator model, which provides a minimal description of synchronization phenomena in complex systems. Section 5.2 presents the formal mathematical definition of the DNM and its medical interpretation, followed by implementation details in Section 5.3 and a presentation of selected simulation results in Section 5.3.4.

5.1 Theoretical Background: The Kuramoto Oscillator Model

To mathematically describe natural or technological phenomena, *coupled oscillators* have proven to be a useful framework [6], for example, to model the relative timing of neural spiking, reaction rates of chemical systems or dynamics of epidemics [6]. In these cases complex networks of coupled oscillators are often capable of bridging microscopic dynamics and macroscopic synchronization phenomena observed in biological systems.

One of the most influential system of coupled oscillators is the *Kuramoto Phase Oscillator Model* which is often used to study how synchronization emerges from simple coupling rules. In the simplest form it consists of N identical, fully connected and coupled oscillators with phase $\varphi_i \in [0, 2\pi),$ for $i \in 1...N$ and an intrinsic frequency ω_i [6]. The dynamics are given by:

$$\dot{\varphi}_i = \omega_i - \frac{\mathrm{K}}{N} \sum_{j=1}^{N} \sin\big(\varphi_i - \varphi_j\big) \tag{1}$$

Here the $\dot{\varphi}$ is used as shorthand notation for the time derivative of the phase $\frac{d\varphi}{dt}$, the instantaneous phase velocity. An additional parameter is the global coupling strength K between oscillators i and j.

The model captures the essential mechanism of self-synchronization, and a fundamental collective transition from disorder to order, that underlie many real world processes, which is the reason the model has attracted so much research. When evolving this system with time, oscillator i's phase velocity depends on each other oscillator j. If $\varphi_j > \varphi_i$ the phase oscillator i accelerates $\dot{\varphi}_i > 0$, if $\varphi_j < \varphi_i$ decelerates. For sufficiently large N the oscillator population can converge towards system-scale states of coherence or incoherence based on the choice of K. Coherent in this case means oscillators synchronize with each other, so they share the same phase and phase velocity, incoherence on the other hand is the absence of synchronization (desynchronized), see Figure 2. Synchronous states can be reached if the coupling is stronger than a certain threshold $\mathrm{K} > \mathrm{K}_c$, the critical coupling strength. In between these two regimes there is a transition-phase of partial synchronization, where some oscillators phase- and frequency-lock and others do not.

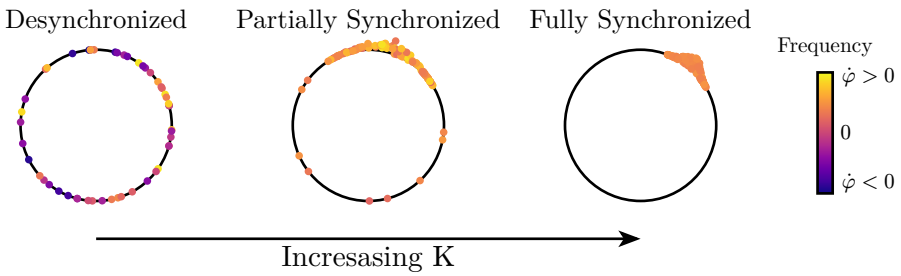

Figure 2: Schematic transition between the two stable regimes for the basic Kuramoto model. From an incoherent system state with desynchronized oscillators (heterogeneous phases and frequencies), to a synchronized system state with phase- and frequency-locked oscillators with increasing coupling strength K).

5.1.1 Extensions to the Kuramoto Model

To more accurately describe real world systems, various extensions of the basic Kuramoto model have been proposed and studied numerically and analytically. Several extensions are directly relevant to the DNM and their definitions and effects on synchronization will be shortly introduced, with additional terms being indicated by the red color:

Phase Lag α introduced in [6] (Kuramoto Sakaguchi 86) , brings a frustration into the synchronization process:

cite

$$\dot{\varphi}_i = \omega_i - \frac{\mathrm{K}}{N}\sum_{j=1}^{N}\sin(\varphi_i - \varphi_j + \alpha) \tag{2}$$

Positive values of α act as an inhibitor of synchronization by shifting the coupling function, so the coupling does not vanish even when the phases align. As a result the critical coupling strength K_c increases with α.

Adaptive coupling $\mathbf{K} \in \mathbb{R}^{N\times N}$ moves from a global coupling strength K for all oscillator pairs to an adaptive coupling strength for each individual pair κ_{ij}:

$$\dot{\varphi}_i = \omega_i - \frac{1}{N}\sum_{j=1}^{N}\kappa_{ij}\sin(\varphi_i - \varphi_j) \tag{3.1}$$

$$\dot{\kappa}_{ij} = -\varepsilon\big(\kappa_{ij} + \sin(\varphi_i - \varphi_j + \beta^{\mu})\big) \tag{3.2}$$

Here adaption rate $0 < \varepsilon \ll 1$ separates the fast moving oscillator dynamics from slower moving coupling adaptivity [34]. Such adaptive couplings have been used to model neural plasticity and learning-like processes in physiological systems [6]. The so called new phase lag parameter β of the adaptation function (also called plasticity rule) plays an essential role. At a value of $\beta^{\mu} = \frac{\pi}{2}$ the coupling, and therefore the adaptivity, is at a maximum positive feedback, strengthening the link κ_{ij} (Hebbian Rule: fire together, wire together [34]) and encouraging synchronization between oscillators i and j. For other values $\beta^{\mu} \neq \frac{\pi}{2}$ the feedback is delayed $\varphi_i^{\mu} - \varphi_j^{\nu} = \beta^{\mu} - \frac{\pi}{2}$ by a phase lag, a value of $\beta^{\mu} = -\frac{\pi}{2}$ we get an anti-Hebbian rule which inhibits synchronization.

Multiplex Networks represent systems with multiple interacting layers. Multiplexing introduces a way how several Kuramoto networks can be coupled via interlayer links:

$$\dot{\varphi}_i^{\mu} = \omega_i - \frac{\mathrm{K}}{N}\sum_{j=1}^{N}\sin(\varphi_i - \varphi_j + \alpha^{\mu\mu}) - \sigma^{\mu\nu}\sum_{\nu=1,\nu\neq\mu}^{L}\sin(\varphi_i^{\mu} - \varphi_i^{\nu} + \alpha^{\mu\nu}) \tag{4}$$

Here μ and ν represent distinct subsystems, and are connected via interlayer coupling weights $\sigma^{\mu\nu}$, acting one-to-one.

These extensions combined serve as the source of dynamics for the DNM and give rise to more intricate system states than the straightforward synchronization in the base model. Even for single layers, non-multiplexed but phase-lagged and adaptively coupled oscillators, one can observe several distinct system states, neither fully synchronized or desynchronized such as phase and frequency-clusters, chimera- and splay states. The emergence of these states depends on the choice of the coupling strength K and the phase-lag parameters α and β.

In the frequency clustered state, the oscillator phases do not synchronize, but several oscillator groups can form that share a common frequency. For the phase-clustered case, the groups additionally synchronize their phase. Frequency clusters often emerge as intermediate regimes between full synchronization and incoherence [35].

Chimera states, a special type of partial synchronization, occur when only a subset of oscillators synchronizes in phase and frequency, while others remain desynchronized. In contrast to "normal" partial synchronization they occur when the coupling symmetry breaks. In splay states, all oscillators synchronize their frequencies but do not their phases, they instead uniformly distribute around the unit circle [34].

The introduction changes the system behavior once more, for example single layers of a multiplexed system can result in the multi-clustered regime for parameters they would not in the monoplexed case. In multiplexed systems it is also possible connected layers end up in different stable state, for example, one in a clustered the other in a splay state.

5.2 Description

Figure bio vs oscillators

The DNM is a **functional** model, that means it **does not try to model things accurately on any cellular, biochemical, or organ level**, it instead tries to model dynamic interactions. At the core, the model does differentiate between two broad classes of cells, introduced in Section 3.2.1, the stroma and the parenchymal cells. It also includes the cell interaction through cytokine proteins and an information flow through the basal membrane. Importantly, the model only handles the case of already infected subjects and tries to grasp if the patients state is prone to a dysregulated host response.

Cells of one type are aggregated into layers, everything associated with parenchymal cells is indicated with an ^{1} superscript and is called the *organ layer*, stroma cells are indicated with ^{2} and is referred to as non specific *immune layer*. Each layer consists of N phase oscillators $\varphi_i^{1/2} \in [0, 2\pi)$. To emphasize again the function aspect of the model: individual oscillators do not correspond to single cells, rather the layer as a whole is associated with the overall state of all organs or immune system functionality respectively.

The metabolic cell activity is modeled by rotational velocity $\dot{\varphi}$ of the oscillators, the faster the rotation, the faster the metabolism. Each layer is fully coupled via an adaptive possibly asymmetric matrix $\mathbf{K}^{1/2} \in [-1, 1]^{N\times N}$ with elements $\kappa_{ij}^{1/2}$, these couplings represent the activity of cytokine mediation. Small absolute coupling values indicate a low communication via cytokines

and grows with larger coupling strength. For the organ layer there is an additional non-adaptive coupling part $\boldsymbol{A}^1 \in [0,1]^{N\times N}$ with elements a_{ij}^1, representing a fixed connectivity within an organ.

The dimensionless system dynamics are described with the following coupled Ordinary Differential Equation (ODE) terms, build on the classical Kuramoto model described in Section 5.1 and its extensions from Section 5.1.1:

$$\dot{\varphi}_i^1 = \omega^1 - \frac{1}{N}\sum_{j=1}^{N}\{(a_{ij}^1 + \kappa_{ij}^1)\sin(\varphi_i^1 - \varphi_j^1 + \alpha^{11})\} - \sigma\sin(\varphi_i^1 - \varphi_i^2 + \alpha^{12}) \tag{5.1}$$

$$\dot{\kappa}_{ij}^1 = -\varepsilon^1(\kappa_{ij}^1 + \sin(\varphi_i^1 - \varphi_j^1 - \beta)) \tag{5.2}$$

$$\dot{\varphi}_i^2 = \omega^2 - \frac{1}{N}\sum_{j=1}^{N}\kappa_{ij}^2\sin(\varphi_i^2 - \varphi_j^2 + \alpha^{22}) - \sigma\sin(\varphi_i^2 - \varphi_i^1 + \alpha^{21}) \tag{5.3}$$

$$\dot{\kappa}_{ij}^2 = -\varepsilon^2(\kappa_{ij}^2 + \sin(\varphi_i^2 - \varphi_j^2 - \beta)) \tag{5.4}$$

Where the interlayer coupling, i.e. a symmetric information through the basal lamina, is modeled by the parameter $\sigma \in \mathbb{R}_{\geq 0}$. The internal oscillator frequencies are modeled by the parameters $\omega^{1/2}$ and correspond to a natural metabolic activity.

Besides the coupling weights in $\mathbf{K}^{1/2}$ the intralayer interactions also depend on the phase lag parameters α^{11} and α^{22} modeling cellular reaction delay. To separate the fast moving oscillator dynamics from the slower moving coupling weights adaption rates $0 < \varepsilon \ll 1$ are introduced. Since the adaption of parenchymal cytokine communication is assumed to be slower than the immune counterpart [25], it is chosen $\varepsilon^1 \ll \varepsilon^2 \ll 1$, which introduces dynamics on multiple timescales.

Lastly, the most influential parameter is β which controls they adaptivity of the cytokines. Because β has such a big influence on the model dynamics it is called the *(biological) age parameter* and summarizes multiple physiological concepts such as age, inflammatory baselines, adiposity, pre-existing illness, physical inactivity, nutritional influences and other common risk factors [26].

All the systems variables and parameters are summarized in | together with their medical interpretation.

why no ref?

Table 1: todo

Symbol	Name	Physiological Meaning
Variables		
φ_i	Phase	Group of cells
$\dot{\varphi}_i$	Phase Velocity	Metabolic activity
κ_{ij}	Coupling Weight	Cytokine activity
Parameters		
α	Phase lag	Metabolic interaction delay
β	Plasticity rule	Combined of risk factors

Symbol	Name	Physiological Meaning
ω	Natural frequency	Natural cellular metabolism
ε	Time scale ratios	Temporal scale of cytokine activity
a_{ij}	Connectivity	Fixed intra-organ cell-to-cell interaction
σ	Interlayer coupling	Interaction between parenchymal and immune cells through the basal lamina
Measures		
s	Standard deviation of frequency (see Equation 11)	Pathogenicity (Parenchymal Layer)

left out superscript for better readability

5.2.1 Pathology in the DNM

A biological organism, such as the human body, can be regarded as a self-regulating system that, under healthy conditions, maintains a homeostatic state [6]. Homeostasis refers to a dynamic but balanced equilibrium in which the physiological subsystems continuously interact to sustain stability despite external perturbations. In the context of the DNM, this equilibrium is represented by a synchronous regime of both layers in the duplex oscillator system. In synchronous states, the organ layer and immune layer exhibit coordinated phase and frequency dynamics, reflecting balanced communication, collective frequency of cellular metabolism and stable systemic function.

Pathology, in contrast, is modeled by the breakdown of the synchronicity and the formation of frequency clusters in the parenchymal layer, i.e. loss of homeostatic balance. In the DNM least one cluster will exhibit increased frequency and one with lower or unchanged frequency. This aligns with medical observation, where unhealthy parenchymal cells change to a less efficient anaerobic glycosis based metabolism, forcing them to increase their metabolic activity to keep up with the energy demand. Remaining healthy cells are expected to stay frequency synchronized to a lower and “healthy” frequency.

There are two more cases, neither fully healthy nor fully pathologic, representing a vulnerable or resilient patient condition. The healthy but vulnerable case corresponds to a splay state, where phases in the parenchymal layer are not synchronized, but the frequencies are, weakening the overall coherence [26]. A resilient state corresponds to cases where both the phase and frequency of the parenchymal layer are synchronized, but the immune layer exhibits both frequency and phase clustering.

5.3 Implementation

For initial value problems of coupled ODE-systems, such as the DNM, analytical solutions rarely exist [26], and if they exists it is mostly for trivial or other special configurations or by applying aggressive simplifications. To solve these kind of systems one traditionally relies on the numerical integration, approximating the analytical solution.

This subsection describes the implementation for the numerical integration of the DNM defined in Equation 5, the choice of initial parameter values and how (de-)synchronicity/disease severity

is quantified. One goal of this implementation is to partly reproduce the numerical results presented in [26], since they will be serving as a basis for following chapters.

5.3.1 Technology and Details

The backbone for the present numerical integration is JAX [36], a Python package for high-performance array computation, similar to NumPy or MATLAB but designed for automatic differentiation, vectorization and Just In Time Compilation (JIT). JIT-compilation and vectorization allow high-level numerical code to be translated to highly optimized accelerator-specific machine code, for example Graphics Processing Unit (GPU). This way, performance benefits of massively parallel hardware can be utilized with minimal extra programming cost. For the actual integration a differential equation solver from diffrax [37] was used, which provides multiple solving schemes fully built on top of JAX.

While [26] uses a fourth-order Runge-Kutta method and a fixed step-size, this implementation[1] uses the Tsitouras 5/4 Runge-Kutta method [38] with adaptive step-sizing controlled by a Proportional-Integral-Derivative (PID) controller. A relative tolerance of 10^{-3} and an absolute tolerance 10^{-6} were chosen, allowing for more efficient integration while keeping an equivalent accuracy. All simulations were carried out in 64-bit floating point precision, necessary for accurate and stable system integration.

Because of the element-wise differences used in the coupling terms $\varphi_i^{1/2} - \varphi_j^{1/2} \in \mathbb{R}^{N\times N}$ the computational cost scales quadratically with the number of oscillators N. These differences are then transformed by the computationally expensive trigonometric sin routine. To accelerate integration, these trigonometric evaluations were optimized following [39]. Terms in the form $\sin(\theta_l - \theta_m)$ were expanded as:

$$\sin(\theta_l - \theta_m) = \sin(\theta_l)\cos(\theta_m) - \cos(\theta_l)\sin(\theta_m) \qquad \forall l, m \in \{1, ..., N\} \tag{6}$$

By caching the terms $\sin(\theta_l)$, $\sin(\theta_m)$, $\cos(\theta_l)$, $\cos(\theta_m)$ once per iteration, the number of trigonometric evaluations per iteration is reduced from $2 \cdot [N(N-1)]$ to $2 \cdot [4N]$, significantly improving performance for mid to large oscillator populations.

Additionally, an alternative implementation based on Lie-algebra formulations was also explored, utilizing their natural representation for rotations in N-D-space. Although theoretically promising in terms of numerical accuracy and integration stability, this approach did not yield practical advantages in performance. Further details on this reformulation are provided in Section 11 .

schreiben

5.3.2 Parameterization and Initialization

The DNM is dimensionless and not bound to any physical scale, that means there is no medical ground truth of parameter values and their choice is somewhat arbitrary. For the present implementation the parameterization is adopted from the original works [25] and [26] since they have already shown desired properties of (de-)synchronization and valid medical interpretations for these parameter choices.

The majority of their parameter choices heavily simplify the model. First of all, the different natural frequencies are treated as equal and are set to 0 giving $\omega^1 = \omega^2 = \omega = 0$, any other

[1] The code is available at https://github.com/unartig/sepsis_osc/tree/main/src/sepsis_osc/dnm

choice of ω just changes the frame of reference (co-rotating frame), the dynamics stay unchanged [26]. The phase lag parameters for the inter layer coupling are both set to $\alpha^{12} = \alpha^{21} = 0$, yielding instantaneous interactions, the intralayer phase lags are set to $\alpha^{11} = \alpha^{22} = -0.28\pi$, which was the prominently used configuration in [26] yielding the desired dynamical properties. The constant intralayer coupling in the parenchymal is chosen as global coupling $a_{ij} = 1 \;\text{ if }\; i \neq j \;\text{ else }\; 0$.

The adaptation rates are chosen as $\varepsilon^1 = 0.03$ and $\varepsilon^2 = 0.3$, creating the two dynamical timescales for slow parenchymal and faster immune cells. The number of oscillators per layer is chosen as $N = 200$ throughout all simulations. To account for the randomly initialized variables, each parameter configuration is integrated for an ensemble of $M = 50$ initializations.

In [26] the influence of parameter values for β and σ was investigated and not constant throughout different simulations, with $\beta \in [0.4\pi, 0.7\pi]$ and $\sigma \in [0, 1.5]$, in this work the interval for β was increased to $[0.0, 1.0\pi]$. An exhaustive summary of all variable initializations and parameter choices can be found in Table 2.

Table 2: Parameterization and initialization of the DNM used for the numerical integration.

Symbol	Value	Symbol	Value
Variables			
φ_i^1	$\sim \mathcal{U}(0, 2\pi)$	$\kappa^1_{i\neq j}$	$\sim \mathcal{U}(-1, 1)$
φ_i^2	$\sim \mathcal{U}(0, 2\pi)$	$\kappa^2_{i\neq j}$	clusters of size C and $1 - C$
Parameters			
M	50	N	200
C	20%		
β	$[0.0, 1.0]\pi$	σ	$[0.0, 1.5]$
α^{11}, α^{22}	-0.28π	α^{12}, α^{21}	0.0
ω_1, ω_2	0.0	A^1	$\mathbb{1} - I$
ε^1	0.03	ε^2	0.3

Non breakable tables?

Initial values for the system variables, i.e. the phases and coupling strengths, were not parametrized explicitly, rather sampled from probability distributions. The initial phases $\varphi(0)_i^{1/2}$ are randomly and uniformly distributed around the unit circle for both layers, i.e. $\varphi(0)_i^{1/2} \sim \mathcal{U}[0, 2\pi)$. The intralayer coupling of the parenchymal layer coupling is also chosen randomly and uniformly distributed in the interval $[-1.0, 1.0]$. Since there is no self-coupling, the diagonal is set to 0.

For the immune layer an initial cytokine activation is models by clustering the initial intralayer coupling matrix. A smaller cluster of $C \cdot N$ oscillators and a bigger cluster of $(1 - C) \cdot N$ cells. Within the clusters oscillators are connected but not between the clusters. Following [26] the cluster size $C \in [0, 0.5]$ was chosen as 0.2, but as their findings suggest the size of the clusters does not have impact on the systems dynamics. Simulations have shown that even without any clustering, meaning $\mathbf{K}^2 = \mathbb{0}$ or $\mathbf{K}^2 = \mathbb{1}$, the dynamics stay unchanged, making this initialization

choice meaning-free, it is stated here just for completeness. An example for initial variable values of a system with $N = 200$ and $C = 0.2$ is shown in Figure 3.

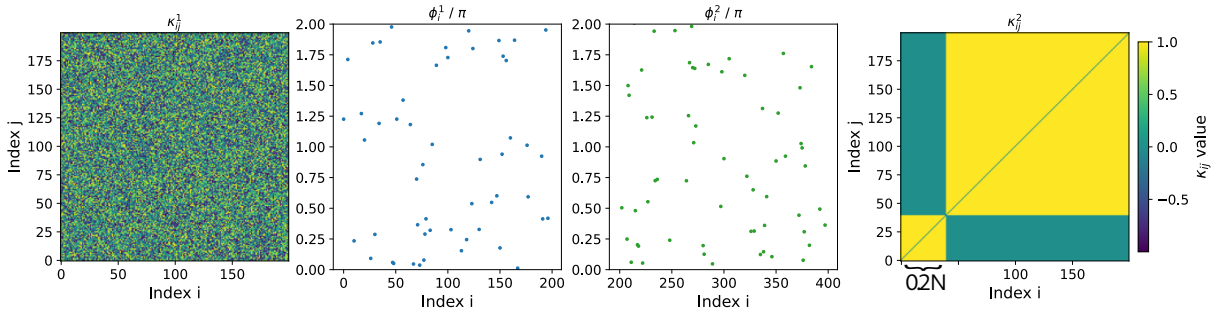

Figure 3: This figure shows the initializations for the variable values of a DNM with $N = 200$ oscillators per layer. The middle two plots show the phases of the oscillators, with φ_i^1 for parenchymal and φ_i^2 for the immune layer, sampled from a uniform random distribution from 0 to 2π. On the left-hand side is the initialization of the parenchymal intralayer coupling matrix $\mathbf{K}^1$ from a uniform distribution in the interval from -1 to 1. On the right-hand side is the two cluster initialization for the coupling matrix $\mathbf{K}^2$ of the immune layer, with a cluster size of $C = 0.2$, where each cluster is intra-connected, but without connections between the clusters.

index for immune

To average out the influence of specific random initial values, simulations are performed for ensembles, combining $m \in 1, 2...M$ ensemble members. Throughout this work an ensemble size of $M = 50$ was used.

5.3.3 Synchronicity Metrics

As introduced in Section 5.1, for the complex Kuramoto networks the synchronization behavior is usually the point of interest, in the following two metrics are introduced, relevant to connect the DNM-dynamics to sepsis. There are two relevant states or system configurations that should be identifiable and quantifiable to allow qualified state analyzes: phase and frequency synchronization, for each a distinct measure is required.

Phase synchronization of a layer is commonly measured by the *Kuramoto Order Parameter* [6]:

$$R_2^{1/2} = \frac{1}{N} \left| \sum_j^N e^{i \cdot \varphi_j^{1/2}(t)} \right| \quad \text{with} \quad 0 \leq R_2^{1/2} \leq 1 \tag{7}$$

where $R_2^{\mu} = 0$ corresponds to total desynchronization, the splay-state and $R_2^{\mu} = 1$ corresponds to fully synchronized state, for convenience from now on the subscript $_2$ is omitted, denoting the Kuramoto Order Parameter simply as $R^{1/2}$.

Frequency synchronization measurements are more involved, as a starting point first the notion of a layers *mean phase velocity* has to be introduced, which can be calculated as follows:

$$\overline{\omega}^{1/2} = \frac{1}{N} \sum_j^N \dot{\varphi}_j^{1/2} \tag{8}$$

The original definition in [25] and [26] uses an approximated version using the oscillators mean velocity. This is likely because they were not able to recover the actual derivatives $\dot{\varphi}_i^{1/2}$ from their integration scheme and had to work with the phases $\varphi_i^{1/2}$ instead:

$$\langle \dot{\varphi}_j^{1/2} \rangle = \frac{\varphi_j^{1/2}(t+T) - \varphi_j^{1/2}(t)}{T} \tag{9.1}$$

$$\overline{\omega}^{1/2} = \frac{1}{N} \sum_j^N \langle \dot{\varphi}_j^{1/2} \rangle \tag{9.2}$$

for some averaging time window T. But since their choice of T is not documented while having substantial influence on the calculation the direct calculation was preferred.

One can now calculate the standard deviation of the mean phase velocities:

$$\sigma_\chi\left(\overline{\omega}^{1/2}\right) = \sqrt{\frac{1}{N} \sum_j^N \left(\langle \dot{\varphi}_j^{1/2} \rangle - \overline{\omega}^{1/2} \right)^2} \tag{10}$$

Where $\sigma_\chi = 0$ indicates full frequency synchronization and growing values indicate desynchronization and/or clustering. But non-zero values only reveal that there is some desynchronization of the frequency, but it remains unknown if it is clustered, multi-clustered or fully desynchronized.

Since there are multiple ensemble members m for the same parameterization, and it expected that different initialization, even though equally parameterized, can exhibit dissimilar behaviors, one can also calculate the *ensemble averaged standard deviation of the mean phase velocity*:

$$s^{1/2} = \frac{1}{M} \sum_m^M \sigma_\chi\left(\overline{\omega}_m^{1/2}\right) \tag{11}$$

In [26] it was shown numerically that the quantity $s^{1/2}$ is proportional to the fraction of ensemble members that exhibit frequency clusters containing at least one oscillator. This makes s^1 a viable measure for pathology, as increasing values of s^1 or increasing system incoherence then indicate more dysregulated host responses and consequently higher risks of multiple organ failure.

5.3.4 Simulation Results

The original findings of [26] identify β, the combined age parameter, and σ, the interlayer coupling strength which models the cytokine activity, as naturally important parameters in order to understand underlying mechanisms of sepsis progression. In the following subsection multiple simulation results are presented, starting with time-snapshots for different parameterization and initializations. Afterward, the transient and temporal behavior of the metrics $s^{1/2}$ and $R^{1/2}$ is for the same parameterization, as well as the introduction of the β, σ phase space of these metrics.

In Figure 4 snapshots of the system variables are shown for different parameterization, differing only in the choice β and σ, configurations A, B, C and D are listed in Table 3, other parameters are shared between the configurations and are stated in Table 2. Each configuration is expected to represent a single patient state.

All following results are for a system with $N = 200$ oscillators, and snapshots taken at time $t = 2000$, the end of the integration time, and show the stationary values at that time point.

Table 3: Specific β-σ combinations to illustrate simulation results.

	A	B	C	D
β	0.5π	0.58π	0.7π	0.5π
σ	1.0	1.0	1.0	0.2

In Figure 4 the left-most columns depicts the coupling matrices for the organ layer $\mathbf{K}^1$ followed by two columns showing the phase velocities for each oscillator $\dot{\varphi}_i^{1/2}$ and two columns showing the oscillator phases each layer $\varphi_i^{1/2}$. The right-most column shows the coupling matrix for the immune layer $\mathbf{K}^2$. Each layer is sorted first from lowest to highest frequency and secondary by lowest to highest phase for better clarity. Rows C and C' share the same parameterization but are different samples from the same initialization distributions.

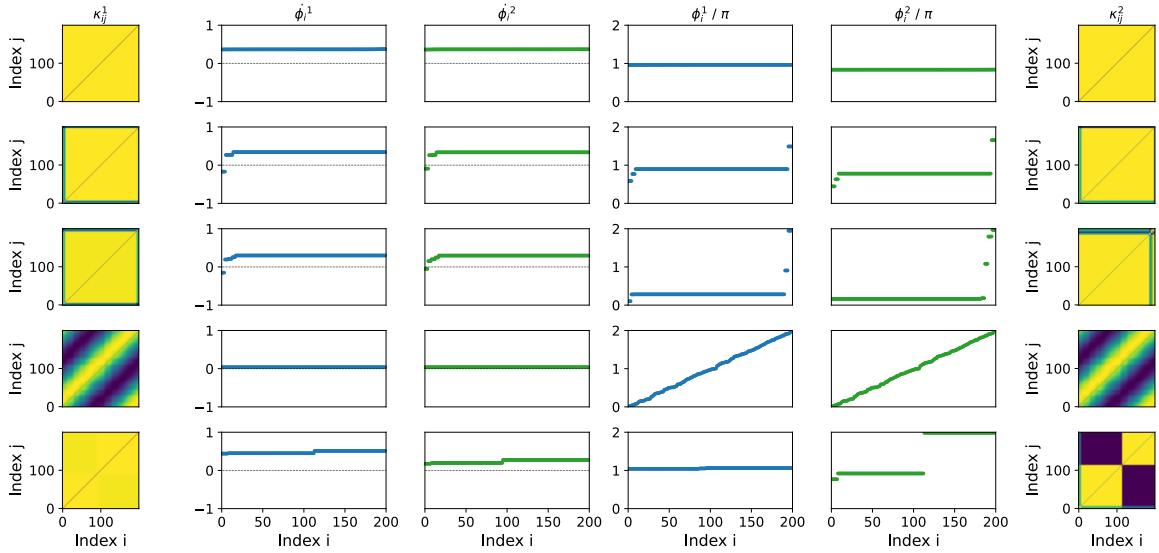

Figure 4: Snapshots of different DNM parametrization and initialization. Configuration A can be regarded as healthy, with phases and frequencies being fully synchronized. In contrast, B and C are pathologic, due to their clustering in $\dot{\varphi}^1$. Configuration C' corresponds to a vulnerable state, because of uniformly distributed phases (splay state). Lastly, D is regarded as resilient, since the phases exhibit clustering, but the frequencies $\dot{\varphi}^1$ are synchronized.

K colorbar

Row A in Figure 4 is fully synchronized/coherent since it not only has the frequencies synchronized but also the phases and can therefore interpreted as healthy. The coherence can also be seen in the fully homogeneous coupling matrices where both $\mathbf{K}^{1/2}$ show the same coupling strength for every oscillator pair. The rows B and C in contrast show signs of a pathological state, here both the frequencies three and phases have four distinct clusters respectively. The clusters are also visible in the coupling matrices, where the coupling strength differs based on the cluster. The row for C', even though having the same parameterization as C, can be regarded vulnerable, since the phases uniformly distribute in the $[0, 2\pi)$ interval ($R^{1/2} = 0$), while the frequencies are synchronized. Coupling matrices for C' show traveling waves, which are characteristic for splay states. Observing different results for different initializations justifies the introduction of ensembles. Lastly row D shows a resilient state, where the phases are clustered while the frequencies are synchronized.

which is stronger

For the next result, the ensembles were introduced, every configuration of A, B, C and D was simulated for $M = 50$ different initializations over an interval of $t = 2000$. The two left-most columns show the standard deviation of the mean phase velocities $s^{1/2}$ for each ensemble member m. The plots show the temporal evolution of metrics for quantifying phase and frequency coherence, with the two right-most columns of Figure 5 show the temporal behavior of the Kuramoto Order Parameter for each individual ensemble member $m \in 1, 2...M$. Where lower values for $R^{1/2}$ indicate decoherence in phases, with its minimum $R^{1/2} = 0$ coincides with a splay state, and for $s^{1/2}$ higher values indicate a larger amount of frequency decoherence and clustering.

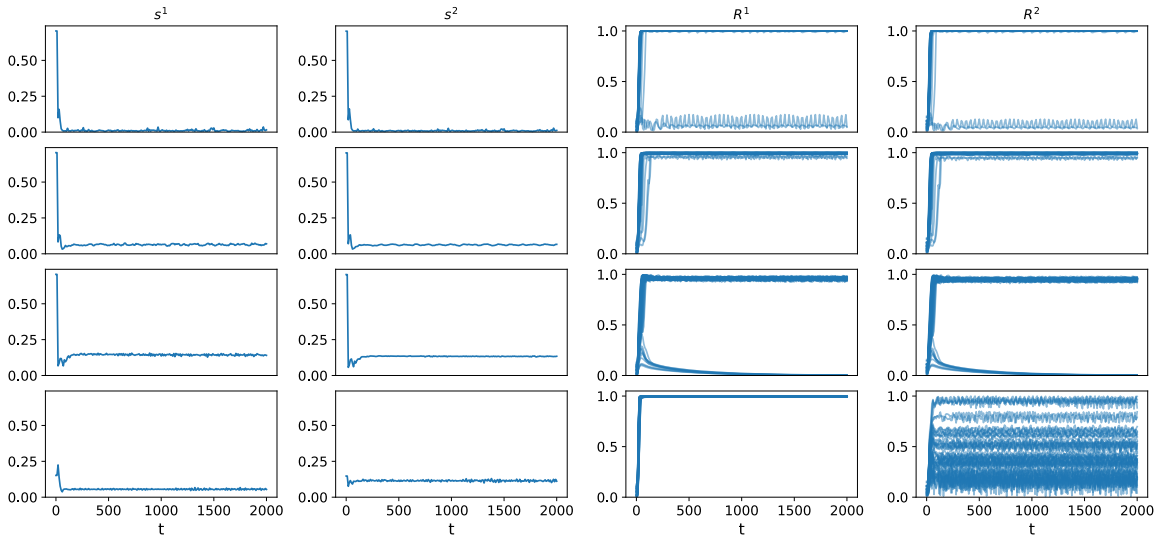

Figure 5: Transient and temporal evolution of the phase- and frequency-synchronization metrics $R^{1/2}$ and $s^{1/2}$, for ensembles of the DNM for the configurations listed in Table 3. Emphasizing the influence of β and σ on the systems synchronization behavior, and presenting different stable emergent system states.

Every ensemble in Figure 5 shows decoherence for early time-points, which is expected for randomly initialized variables, but changes relatively fast through a transient phase $t \in [0.0, 200]$ into systematic stable behavior. The stable states align with the observations made for Figure 4, configuration A has, besides small jitter, mostly synchronized frequencies $s^{1/2} \tilde{=} 0$. Also the phases of configuration A are mostly synchronized with $R^{1/2} \tilde{=} 1$, only two initializations show decoherence and are oscillating between weak clustering and almost full incoherence. Medically this can be interpreted as a low risk of a dysregulated host response for an otherwise healthy response to the initial cytokine activation. For configuration B the amount of incoherence inside the ensemble is clearly visible, with $s^{1/2}$ being positive and some more ensemble members exhibiting clustering, indicated by a Kuramoto Order Parameter slightly less than 1. In configuration C the incoherence is even more prominent, larger $s^{1/2}$ and some ensemble members evolving into a splay state, i.e. $R^{1/2} = 0$. For configuration D the overall phase incoherence is again a bit less compared to C, and lower for the organ compared to the immune layer. The phases are coherent for the organ layer but seem almost chaotic for the immune layer, some are synchronized, while others are clustered, in a chimera or almost splay-like state. Over the whole simulation period, the coherency in the immune layer seems not to fully stabilize, rather oscillate around an attractor.

Each of the configurations only differs in the parameter choices for β and σ, yet they evolve into unique and distinct system states. To put these four specific configurations into broader perspective, a grid of β and σ was simulated, in the interval $\beta \in [0, 1]$ with a grid resolution of 0.01 and $\sigma \in [0, 1.5]$ with a resolution of 0.015, creating a grid of $10,000$ points. In Figure 6 the metric $s^{1/2}$ is shown in the $\beta - \sigma$ phase space for both layers in the first row, where brighter colors indicate a larger risk of frequency desynchronization, or risk of dysregulated immune response. The second row shows the ensemble mean over $\overline{R}^{1/2}$, i.e. $\overline{R}^{1/2} = \frac{1}{M}\sum_m^M R_m^{1/2}$, with $M = 50$, where darker colors indicate larger phase desynchronization. The white rectangle indicates the simulated region in [26], $\beta \in [0.4, 0.7]$ and $\sigma \in [0, 1.5]$ for reference. Coordinates of the configurations A, B, C, and D are also labeled.

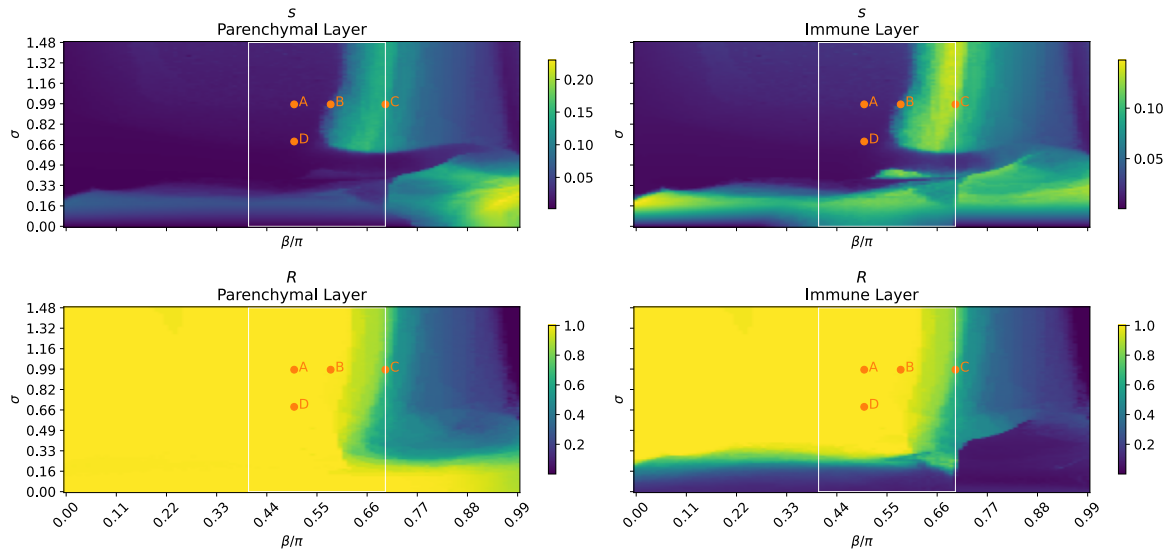

Figure 6: Phase space of the parameters β and σ and illustrating the broader picture their influence on the frequency and phase synchronization of the DNM. White rectangle indicates the grid-limits of the original publication [26].

Generally there is a similarity between phase and frequency desynchronization but no full equality, meaning there are parameter regions where the phase is synchronized and frequency desynchronized and vice versa. Another observation, that smaller values of $\beta < 0.55$ correspond to less desynchronization and stronger coherence, which is in line with the medical interpretation of β where smaller values indicate a younger and more healthy biological age. When crossing a critical value of $\beta_c \tilde{=} 0.55$ for the frequency and $\beta_c \tilde{=} 0.6$ for the phases, the synchronization behavior suddenly changes and tends towards incoherence, clustering and pathological interpretations.

For small values of $\sigma < 0.5$ the frequency synchronization and $\sigma < 0.25$ for the phase synchronization, the behavior significantly differs between immune and organ layer. The immune layer tends to fully desynchronize, instead the organ layer only the frequency desynchronizes for larger $\beta > 0.7$. With larger values of $\sigma > 0.5$ the dynamics more or less harmonize between layers and metrics and are mostly depend on β.

5.4 Why care about the DNM?

Mechanistic baseline Constraint setting

not a sequence

6 Method (Latent Dynamics Model)

This chapter introduces the methodological framework used to address the first research question stated in Section 4:

Usability of the DNM: How and to what extent can the ML-determined trajectories of the DNM be used for detection and prediction, especially of critical infection states and mortality.

To investigate this, a deep learning pipeline has been developed, in which the DNM is embedded as central part. Instead of predicting the sepsis directly, the two components, Suspected Infection and increase in SOFA scores are predicted as direct proxies creating more interpretable results. The main idea is to utilize the parameter level synchronization dynamics of the DNM, particularly β and σ, to provide a starting ground for short-term machine learned organ system trajectories of real patients. The complete architecture, consisting of the DNM and additional auxiliary modules, whole will be referred to as the Latent Dynamics Model (LDM) from now on.

This chapter proceeds with the prediction task to be reiterated formally and the introduction of desired prediction properties, and justification of modeling choices. Afterwards, the individual modules of the LDM will be discussed and focusing on what purpose each serves and how it is integrated into the broader system.

ref sections

6.1 Formalizing the Prediction Task

In automated clinical prediction systems, a patient is typically represented through their Electronic Health Record (EHR). Where the EHR aggregates multiple clinical variables, such as laboratory biomarker, for example from blood or urine tests, or physiological scores and, further demographic information, e.g. age and gender. Using the information in the EHR, the objective is to estimate the patient's risk of developing sepsis in the near future.

6.1.1 Patient Representation

Let $t = 0$ be an arbitrary chosen time-point of a patients ICU-stay and the available EHR at that time consisting of n variables. After imputation of missing values, normalization, and encoding of non-numerical quantities, each variable μ_j is mapped to a numerical value:

$$\mu_j \in \mathbb{R}, \;\; j = 1, ..., n \tag{12}$$

These values are collected into a column-vector:

$$\boldsymbol{\mu} = (\mu_1, ..., \mu_n)^T \in \mathbb{R}^n \tag{13}$$

which is fully describing the current physiological state of the ICU-patient.

6.1.2 Modeling the Sepsis-3 Target

The goal is calculate the risk of developing a septic condition given $\boldsymbol{\mu}$ in the next T future time-steps. This risk is introduced in the Sepsis-3 definition, which requires both suspected infection and multi-organ failure. Defining the *sepsis onset event* S as the occurrence of the Sepsis-3 criteria at any time point within the window $t = 1, ..., T$:

$$S_{1:T} \coloneqq \bigcup_{t=1}^{T} (A_t \cap I_t) \tag{14}$$

Here $A_t = \{\Delta O_t > 2\}$, is denoting an acute change in organ function, with O_t being the SOFA-score and $\Delta O_t = O_t - O_{t-1}$ the change in SOFA-score with respect to the previous time-step. I_t is an event indicator for a Suspected Infection at time t. The target probability given the current EHR is then:

$$\Pr(S_{1:T}|\boldsymbol{\mu}) = \Pr\left(\bigcup_{t=1}^{T} (A_t \cap I_t) \mid \boldsymbol{\mu} \right) \tag{15}$$

6.1.3 Heuristic Scoring and Risk Estimation

The direct estimation of the conditional probability $P(S_{1:T}|\boldsymbol{\mu})$ is computationally and statistically challenging due to the temporal dependency between the binary Sepsis-3 criteria. To make the prediction of this probability more tractable but still connect the statistical model to the clinical definition the following assumptions and modeling choices are made resulting in a *heuristic risk score* $\tilde{S}$.

For small T, relative to the total SI-window of 72 h, I_t is approximated as constant over the sequence: $\tilde{I} \coloneqq I_t$ for $t = 1, ..., T$. This binary variable serves as a time-invariant proxy for the presence of a Suspected Infection and can be estimated from $\boldsymbol{\mu}$.

The events A_t are statistically independent across time steps. This is necessary to aggregate the risk across time-points:

$$\Pr(A_{1:T}) = 1 - \prod_{t=1}^{T} \Pr(A_t) \tag{16}$$

. Instead of predicting $\Pr(A_{1:T})$ directly, first the SOFA-score for each time-step $\hat{O}_t$ is estimated from $\boldsymbol{\mu}$. These estimated scores are then used to create a non-linear summary statistic $\tilde{A}$ that relates to the formula of the probability of a union of events:

$$\tilde{A} = 1 - \prod_{t=1}^{T} \text{sigmoid}\Big(s\Big(\hat{O}_t - \hat{O}_{t-1} - d\Big)\Big) \tag{17}$$

With d and s being a calibration threshold and scale respectively. In the original Sepsis-3 definition d is chosen as two. This risk function is used as a summary statistic for the overall risk of SOFA-score increase within the window.

The high-dimensional $\boldsymbol{\mu}$ has now been condensed into two clinically motivated summary statistics $\tilde{A}$ and $\tilde{I}$. The final sepsis risk is then estimated by combining these features using a Generalized Linear Model (GLM). Given the two predicted binary event indicators the estimated probability of true sepsis onset is modeled:

$$S_{1:T} \approx \tilde{S} = \text{sigmoid}\Big(\gamma_0 + \gamma_1 \tilde{A} + \gamma_2 \tilde{I} + \gamma_{12} \tilde{A}\tilde{I}\Big) \tag{18}$$

The interaction term $\tilde{A}\tilde{I}$ is essential as the formal Sepsis-3 definition is based of the conjunction of the two events.

Coefficients $\boldsymbol{\gamma} = (\gamma_0, \gamma_1, \gamma_2, \gamma_{12})^T$ again can be calibrated from $\boldsymbol{\mu}$. It is important to note that $\tilde{S}$ is **not a calibrated probability** but a heuristically derived and empirical risk score based on the Sepsis-3 definition, serving as proxy to the real event probability $P(S_{1:T}|\boldsymbol{\mu})$.

6.2 Architecture

To estimate the components $\tilde{A}$ and $\tilde{I}$ from $\boldsymbol{\mu}$ two Deep Learning modules have been designed. A third module to calibrate the final risk score S from the components relies on more traditional solving of the non-linear function. Each module is introduced in the following subsections on a more technical level.

6.2.1 DNM as SOFA Surrogate

Recalling that the pathological organ conditions are characterized within the DNM by frequency clustering in the parenchymal layer. The amount of frequency desynchronization measured by the ensemble average standard deviation of the mean phase velocity s^1 naturally function as a proxy for a patients SOFA-score. Increasing values of s^1 indicate a higher SOFA-score and a worse condition of the patients organ system.

Numerical integration of the DNM equations for a given parameter pair (β, σ) yields the corresponding SOFA estimate:

$$\hat{O}_t = s^1(\beta_t, \sigma_t) \tag{19}$$

The complete SOFA predictor module is composed of multiple smaller submodules, described below, where this way of generating SOFA-score estimates is used.

6.2.2 Infection Indicator Module

The first module of the LDM estimates the presence of a SI, represented by the binary indicator $\tilde{I}$. Given N pairs of EHR vectors and ground truth SI-indicator

$$\left(\boldsymbol{\mu}_i, \tilde{I}_i\right), i = 1...N \tag{20}$$

a parameterized non-linear function

$$f_\theta : \mathbb{R}^n \to [0, 1] \tag{21}$$

is trained to map the patients physiological state to an estimated probability of suspected infection:

$$\hat{I} = f_\theta(\boldsymbol{\mu}) \tag{22}$$

The model is implemented as a supervised neural network optimized with gradient descent. To fit model, the Binary Cross Entropy (BCE)-loss which measures the distance between true label y_i and the predicted label $\hat{y}_i$:

$$BCE(y, \hat{y}) = -\frac{1}{N}\sum_{i=1}^{N}[y_i \log(\hat{y}_i) + (1 - y_i)\log(1 - \hat{y}_i)] \tag{23}$$

is minimized during training. The resulting estimator provides a stable time-invariant proxy for suspected infection over the short prediction horizon.

6.2.3 SOFA Predictor Module

As discussed in Section 6.1.3 the summarized organ-condition statistic $\tilde{A}$ depends on estimates SOFA-scores $\hat{O}$ at future time steps. These scores are obtained through a multi-stage process that integrates the dynamics of the DNM with learned patient-specific latent representations.

6.2.3.1 Latent Parameter Encoder

To connect the high-dimensional EHR to the dynamical regime of the DNM, a neural encoder:

$$g_\theta : \mathbb{R}^n \to \mathbb{R}^2 \tag{24}$$

maps the patient state to a two-dimensional latent vector

$$\hat{z} = \left(\hat{z}_\beta, \hat{z}_\sigma\right) = g_\theta(\boldsymbol{\mu}) \tag{25}$$

This embedding locates the patient within a physiologically meaningful region of the DNM parameter space. The pair $\hat{z}$ provides the initial condition for short-term dynamical organ condition forecasting.

In addition, the encoder outputs another vector with dimension $h \ll n$ that should compress expected temporal evolution of $\hat{z}$. This vector $\boldsymbol{h} \in \mathbb{R}^h$ is referred to as the hidden state.

Since both output of the function g_θ mark the initial step of the prediction horizon, they receive a 0 as subscript $\hat{\boldsymbol{z}}_0$ and $\boldsymbol{h}_0$.

6.2.3.2 Recurrent Parameter Dynamics

Since the heuristic SOFA risk $\tilde{I}$ depends on the evolution of organ function, it is necessary to estimate not only the initial state $\hat{z}_0$ but also its evolution. For this purpose a neural recurrent function:

$$\hat{\boldsymbol{z}}_t = r_\theta(z_{t-1}, h_t), t = 1, ..., T \tag{26}$$

is trained to propagate the latent DNM parameters forward in time. This model captures how patient physiology modulates the drift of the DNM parameters and therefore how the organ's synchrony pattern evolves over the prediction horizon. This recurrent mechanism captures how the underlying physiology influences the drift of the DNM parameters, and therefore how the level of synchrony changes across the prediction horizon.

6.2.3.3 Decoder

To encourage a semantically structured latent space and prevent the encoder from collapsing to arbitrary parameter configurations, a decoder module is added as an auxiliary regularization component. As a regularization, and to strengthen semantic meaningful positioning of the embedded EHR a decoder The decoder attempts to reconstruct selected clinically relevant EHR features from the latent representation

$$\hat{\boldsymbol{\mu}} = d_{\theta(\hat{\boldsymbol{z}})} \tag{27}$$

ensuring that nearby points in the latent (β, σ)-space correspond to physiologically similar patient states. This regularization promotes a meaningful alignment between EHR-derived embeddings and the DNM's dynamical landscape.

6.2.3.4 Representation Learning

6.2.3.5 Semantics and Latent Spaces

6.2.3.6 Autoregressive Prediction

6.3 The actual implementation

6.3.1 The Lookup (FSQ)

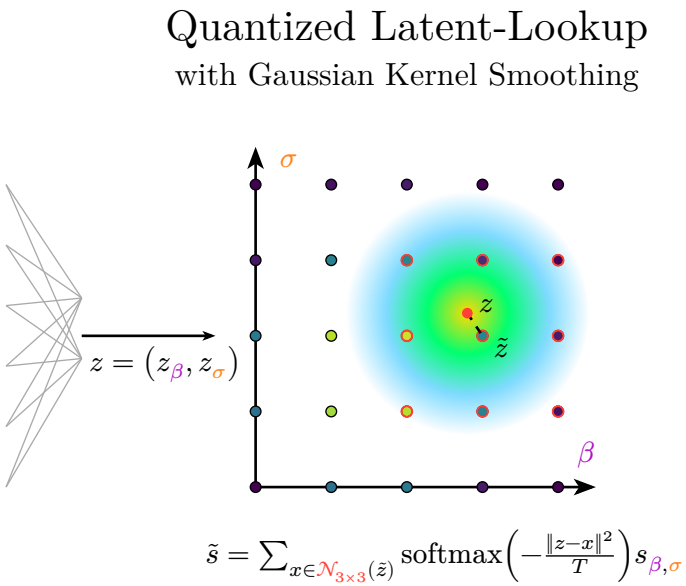

Fix the edges

6.3.2 Combining the building blocks

For a general model setup, the latent space $z = (a^1, \sigma, \alpha, \beta, \omega^1, \omega^2, \frac{C}{N}, \varepsilon^1, \varepsilon^2)$ represents the parameter of the dynamic network model, so we have

$$z \in \mathbb{R}^d \quad \text{with} \quad d = 9 \tag{28}$$

As shown in the supplemental material of [26], for example, the parameter α exhibits a π-periodicity, allowing to reduce the effective parameter space by constraining certain parameters with upper and lower bounds. These bounds are omitted here for simplicity but are included in . To further reduce the latent space z, the we keep $a^1, \omega^1, \omega^2, \frac{C}{N}, \varepsilon^1$ and ε^2 fixed. The reduced latent space $z' = (\sigma, \alpha, \beta)$:

table

$$z' \in \mathbb{R}^{d'} \quad \text{with} \quad d' = 3 \tag{29}$$

where both alpha and beta exhibit a periodic behavior Each point in the latent space z_j can be categorized as either of *healthy*, *vulnerable* or *pathological*.

We relate high-dimensional physiological observations (e.g. samples from the MIMIC-III database) to the latent space via:

$$x_j = f(z_j) + \varepsilon \tag{30}$$

where f is unknown an unknown function and ε the measurement noise. Note that different observations x_j can be mapped to the same classification, as for the latent space. We define two the two class mappings Q and R:

$$Q(x_j) = c_j = R(z_j) \quad \text{where} \quad x_j = f(z_j) + \varepsilon \tag{31}$$

mapping observations and the latent representation to a shared class label c. To make things more complicated, R does not directly act on z, but rather the metrics derived from the solution to a dynamical system (initial value problem) (Equation 5) parameterized by z. The metrics are detailed in.

In the setting of structured latent variational learning we want to approximate an encoder $q(z|x)$ to infer the latent variables from observed data X and the class.

How to structure the latent space? Binary classification (sepsis, no sepsis) may not provide enough information to accurately structure the latent space. The options:

- Add more classes like resilient/vulnerable… maybe even the full spectrum?
  - need to be modeled by R

For the cohort extraction and SOFA calculation I use [40] and [41]. The nice thing is we could interpret larger SOFA scores (> 3) as the vulnerable state introduced by [26]. Increases in SOFA score ≥ 2 could then be used as definition for sepsis.

mapping not really clear, which metrics correspond to sofa/infection

YAIB [41] and other resources care about the "onset" of infection and sepsis [42]. For sepsis this isn't really problematic since we could use the "state transitions" as indicators. But for the suspected infection it is problematic, maybe use si_upr and si_lwr provided by [40] (https://eth-mds.github.io/ricu/reference/label_si.html). These would be 48h - SI - 24h adapted from [43], maybe a bit too much.

7 State of the Art

7.1 Model Based Methods

7.2 Data Based Methods

7.2.1 Selected Works

8 Experiments

8.1 Task - Definition of Ins and Outs

8.2 Data

Figure 8: Sets of [41]

RICU and YAIB use delta_cummin function, i.e. the delta SOFA increase is calculated with respect to the lowest observed SOFA to this point.

8.2.1 MIMIC-III/IV

8.2.2 YAIB + (Further) Preprocessing

8.2.2.1 ricu-Concepts

8.3 Metrics (How to validate performance?)

9 Results

10 Conclusion

11 Appendix

Category	Indicator	1	2	3	4
Respiration	PaO_2/FiO_2 [mmHg]	< 400	< 300	< 200	< 100
	Mechanical Ventilation			yes	yes
Coagulation	Platelets $[\times \frac{10^3}{mm^3}]$	< 150	< 100	< 50	< 20
Liver	Bilirubin $[\frac{mg}{dl}]$	1.2-1.9	2.0-5.9	6.0-11.9	> 12.0
Cardiovascular[2]	MAP [mmHg]	< 70			
	or Dopamine		≤ 5	> 5	> 15
	or Dobutamine		any dose		
	or Epinephrine			≤ 0.1	> 0.1
	or Noepinephrine			≤ 0.1	> 0.1
Central Nervous System	Glasgow Coma Score	13-14	10-12	6-9	< 6
Renal	Creatinine $[\frac{mg}{dl}]$	1.2-1.9	2.0-3.4	3.5-4.9	> 5.0
	or Urine Output $[\frac{ml}{day}]$			< 500	< 200

caption

[2] Adrenergica agents administered for at least 1h (doses given are in [µg/kg · min]

Bibliography

[1] K. E. Rudd and et al., "Global, regional, and national sepsis incidence and mortality, 1990–2017: analysis for the Global Burden of Disease Study," *The Lancet*, vol. 395, no. 10219, pp. 200–211, 2020, doi: 10.1016/S0140-6736(19)32989-7.

[2] E. C. van der Slikke, A. Y. An, R. E. Hancock, and H. R. Bouma, "Exploring the pathophysiology of post-sepsis syndrome to identify therapeutic opportunities," *EBioMedicine*, vol. 61, p. 103044, 2020, doi: 10.1016/j.ebiom.2020.103044.

[3] C. Fleischmann-Struzek, D. Schwarzkopf, and K. Reinhart, "Inzidenz der Sepsis in Deutschland und weltweit: Aktueller Wissensstand und Limitationen der Erhebung in Abrechnungsdaten," *Medizinische Klinik - Intensivmedizin und Notfallmedizin*, vol. 117, no. 4, pp. 264–268, May 2022, doi: 10.1007/s00063-021-00777-5.

[4] M. Singer *et al.*, "The Third International Consensus Definitions for Sepsis and Septic Shock (Sepsis-3)," *JAMA*, vol. 315, no. 8, pp. 801–810, Feb. 2016, doi: 10.1001/jama.2016.0287.

[5] C. W. Seymour *et al.*, "Time to Treatment and Mortality during Mandated Emergency Care for Sepsis," *The New England Journal of Medicine*, vol. 376, pp. 2235–2244, June 2017, doi: 10.1056/NEJMoa1703058.

[6] Max, "Placeholder."

[7] J. L. Vincent *et al.*, "The SOFA (Sepsis-related Organ Failure Assessment) score to describe organ dysfunction/failure. On behalf of the Working Group on Sepsis-Related Problems of the European Society of Intensive Care Medicine," *Intensive care medicine*, vol. 22, no. 7, pp. 707–710, 1996.

[8] A. E. W. Johnson *et al.*, "A Comparative Analysis of Sepsis Identification Methods in an Electronic Database," *Critical Care Medicine*, vol. 46, no. 4, pp. 494–499, Apr. 2018, doi: 10.1097/CCM.0000000000002965.

[9] N. Bennett, D. Plečko, and I.-F. Ukor, "Sepsis 3 label — sep3." 2025.

[10] R. Moreno *et al.*, "The Sequential Organ Failure Assessment (SOFA) Score: has the time come for an update?," *Critical Care*, vol. 27, no. 1, p. 15, Jan. 2023, doi: 10.1186/s13054-022-04290-9.

[11] P. Vaňhara, M. Sedláčková, I. Lauschová, S. Čech, and A. Hampl, *Guide to General Histology and Microscopic Anatomy*. Brno, Czech Republic (Implied by Masaryk University Press): Masaryk University Press, 2020, p. 61. [Online]. Available: https://directory.doabooks.org/handle/20.500.12854/96930

[12] A. M. Honan and Z. Chen, "Stromal Cells Underlining the Paths From Autoimmunity, Inflammation to Cancer With Roles Beyond Structural and Nutritional Support," *Frontiers in Cell and Developmental Biology*, 2021, doi: 10.3389/fcell.2021.658984.

[13] S. Fischer and E. Deindl, "State of the Art of Innate Immunity - An Overview," *Cells*, vol. 11, p. 2705, 2022, doi: 10.3390/cells11172705.

[14] D. Jarczak, S. Kluge, and A. Nierhaus, "Sepsis—Pathophysiology and Therapeutic Concepts," *Frontiers in Medicine*, 2021, doi: 10.3389/fmed.2021.628302.

[15] J. Zhang and J. An, "Cytokines, inflammation, and pain," *Int Anesthesiol Clin*, vol. 45, no. 2, pp. 27–37, 2007, doi: 10.1097/AIA.0b013e318034194e.

[16] R. V. House and J. Descotes, Eds., *Cytokines in Human Health: Immunotoxicology, Pathology, and Therapeutic Applications*, 1st ed. in Methods in Pharmacology and Toxicology. Totowa, N.J.: Humana Press, 2007.

[17] D. Jarczak and A. Nierhaus, "Cytokine Storm—Definition, Causes, and Implications," *International Journal of Molecular Sciences*, vol. 23, no. 19, 2022, doi: 10.3390/ijms231911740.

[18] J. Lamsfus-Prieto, R. de Castro-Fernández, A. Hernández-García, and G. Marcano-Rodriguez, "Prognostic value of gasometric parameters of carbon dioxide in resuscitation of septic patients. A bibliography review," *Revista Española de Anestesiología y Reanimación (English Edition)*, vol. 63, no. 4, pp. 220–230, 2016, doi: https://doi.org/10.1016/j.redare.2015.11.003.

[19] L. La Via *et al.*, "The Global Burden of Sepsis and Septic Shock," *Epidemiologia*, vol. 5, no. 3, pp. 456–478, 2024, doi: 10.3390/epidemiologia5030032.

[20] S. Ein Alshaeba, E. A. Marhoffer, J. L. Holleck, J. Theise-Toupal, A. A. Grimshaw, and C. G. Gunderson, "The Effect of Early Warning Systems for Sepsis on Mortality: A Systematic Review and Meta-analysis," *Journal of General Internal Medicine (J GEN INTERN MED)*, vol. 40, pp. 3463–3468, 2025, doi: 10.1007/s11606-025-09569-5.

[21] G. A. Westphal *et al.*, "Early detection strategy and mortality reduction in severe sepsis," *Revista Brasileira de Terapia Intensiva (Rev Bras Ter Intensiva)*, vol. 21, no. 2, pp. 113–123, June 2009.

[22] G. P. Dobson, H. L. Letson, and J. L. Morris, "Revolution in sepsis: a symptoms-based to a systems-based approach? ," *Journal of Biomedical Science (J Biomed Sci)*, vol. 31, no. 1, p. 57, 2024, doi: 10.1186/s12929-024-01043-4.

[23] B. Eini-Porat, O. Amir, D. Eytan, and U. Shalit, "Tell me something interesting: Clinical utility of machine learning prediction models in the ICU," *Journal of Biomedical Informatics*, vol. 132, p. 104107, 2022, doi: 10.1016/j.jbi.2022.104107.

[24] P. C. Ivanov, "The New Field of Network Physiology: Building the Human Physiolome," *Frontiers in Network Physiology*, 2021, doi: 10.3389/fnetp.2021.711778.

[25] J. Sawicki, R. Berner, T. Löser, and E. Schöll, "Modeling Tumor Disease and Sepsis by Networks of Adaptively Coupled Phase Oscillators," *Frontiers in Network Physiology*, vol. 1, 2022, doi: 10.3389/fnetp.2021.730385.

[26] R. Berner, J. Sawicki, M. Thiele, T. Löser, and E. Schöll, "Critical Parameters in Dynamic Network Modeling of Sepsis," *Frontiers in Network Physiology*, vol. 2, 2022, doi: 10.3389/fnetp.2022.904480.

[27] R. E. Callard, A. J. T. George, and J. Stark, "Cytokines, chaos, and complexity," *Immunity*, vol. 11, no. 5, pp. 507–513, Nov. 1999, doi: 10.1016/s1074-7613(00)80125-9.

[28] A. Schuurman, P. Sloot, W. Wiersinga, and et al., "Embracing complexity in sepsis," *Crit Care*, vol. 27, no. 1, p. 102, 2023, doi: 10.1186/s13054-023-04374-0.

[29] A. C. Guyton, T. G. Coleman, and H. J. Granger, "Circulation: overall regulation," *Annu Rev Physiol*, vol. 34, pp. 13–46, 1972, doi: 10.1146/annurev.ph.34.030172.000305.

[30] R. P. Bartsch, A. Y. Schumann, J. W. Kantelhardt, T. Penzel, and P. C. Ivanov, "Phase transitions in physiologic coupling," *Proc Natl Acad Sci U S A*, vol. 109, no. 26, pp. 10181–10186, June 2012, doi: 10.1073/pnas.1204568109.

[31] K. Lehnertz, T. Rings, and T. Bröhl, "Time in Brain: How Biological Rhythms Impact on EEG Signals and on EEG-Derived Brain Networks," *Front. Netw. Physiol.*, vol. 1, p. 755016, Sept. 2021, doi: 10.3389/fnetp.2021.755016.

[32] M. Madadi Asl, A.-H. Vahabie, A. Valizadeh, and P. A. Tass, "Spike-Timing-Dependent Plasticity Mediated by Dopamine and its Role in Parkinson's Disease Pathophysiology," *Frontiers in Network Physiology*, 2022, doi: 10.3389/fnetp.2022.817524.

[33] N. Sinha, R. B. Joshi, M. R. S. Sandhu, T. I. Netoff, H. P. Zaveri, and K. Lehnertz, "Perspectives on Understanding Aberrant Brain Networks in Epilepsy," *Frontiers in Network Physiology*, 2022, doi: 10.3389/fnetp.2022.868092.

[34] R. Berner, J. Sawicki, and E. Schöll, "Birth and Stabilization of Phase Clusters by Multiplexing of Adaptive Networks," *Phys. Rev. Lett.*, vol. 124, no. 8, p. 88301, Feb. 2020, doi: 10.1103/PhysRevLett.124.088301.

[35] R. Berner, J. Fialkowski, D. Kasatkin, V. Nekorkin, S. Yanchuk, and E. Schöll, "Hierarchical frequency clusters in adaptive networks of phase oscillators," *Chaos: An Interdisciplinary Journal of Nonlinear Science*, vol. 29, no. 10, p. 103134, 2019, doi: 10.1063/1.5097835.

[36] J. Bradbury *et al.*, "JAX: composable transformations of Python+NumPy programs." [Online]. Available: http://github.com/jax-ml/jax

[37] P. Kidger, "On Neural Differential Equations," Doctoral dissertation, 2021.

[38] C. Tsitouras, "Runge–Kutta pairs of order 5 (4) satisfying only the first column simplifying assumption," *Computers & Mathematics with Applications*, vol. 62, no. 2, pp. 770–775, 2011.

[39] T. Böhle, C. Kuehn, and M. Thalhammer, "On the reliable and efficient numerical integration of the Kuramoto model and related dynamical systems on graphs," *International Journal of Computer Mathematics*, vol. 99, no. 1, pp. 31–57, 2022, doi: 10.1080/00207160.2021.1952997.

[40] N. Bennett, D. Plečko, I.-F. Ukor, N. Meinshausen, and P. Bühlmann, "ricu: R's interface to intensive care data," *GigaScience*, vol. 12, p. giad41, 2023.

[41] R. van de Water, H. N. A. Schmidt, P. Elbers, P. Thoral, B. Arnrich, and P. Rockenschaub, "Yet Another ICU Benchmark: A Flexible Multi-Center Framework for Clinical ML," in *The Twelfth International Conference on Learning Representations*, Oct. 2024.

[42] M. Moor, B. Rieck, M. Horn, C. R. Jutzeler, and K. Borgwardt, "Early Prediction of Sepsis in the ICU Using Machine Learning: A Systematic Review," *Frontiers in Medicine*, 2021, doi: 10.3389/fmed.2021.607952.

[43] C. W. Seymour *et al.*, "Assessment of Clinical Criteria for Sepsis: For the Third International Consensus Definitions for Sepsis and Septic Shock (Sepsis-3)," *JAMA*, vol. 315, no. 8, pp. 762–774, 2016, doi: 10.1001/jama.2016.0288.